Icarus 329 (2019) 246–250

Contents lists available at ScienceDirect

Icarus

journal homepage: www.elsevier.com/locate/icarus

The lunar neon exosphere seen in LACE data

Rosemary M. Killen[a,*], David R. Williams[b], Jaekyun Park[c], Orenthal J. Tucker[a], Sang-Joon Kim[c]

[a] NASA Goddard Space Flight Center, Code 695, Greenbelt, MD 20771, USA
[b] NASA Goddard Space Flight Center, Code 690.1, Greenbelt, MD 20771, USA
[c] School of Space Research, Kyung Hee University, Yongin 446-701, Republic of Korea

A B S T R A C T

Using the LACE data from Apollo 17 we have found measured neon densities consistent with the ^{20}Ne surface number densities reported by Cook et al. (2013) for normal conditions, terminator surface densities of 3 (± 1.5) × 10^3 cm^{-3}. These values are almost an order of magnitude less than those reported by Benna et al. (2015) for CME conditions. Using a Monte Carlo model and assuming the normal solar wind and a photoionization lifetime for Ne of 300 days, our result was more consistent with the Benna (2015) result than our measured result. Two lunations showed an increase in Ne during the night, consistent with the simulation, but two of the lunations showed a decrease in surface number density through the night. We have shown that explaining the Ne distribution is not as simple as assuming dynamic equilibrium with the solar wind and an exosphere accommodated to the local surface temperature.

1. Introduction

Apollo 17 carried a miniature mass spectrometer, called the Lunar Atmospheric Composition Experiment (LACE), to the Moon as part of the Apollo Lunar Surface Experiments Package (ALSEP) to study the composition and variations in the lunar atmosphere. The instrument was deployed in the Taurus-Littrow Valley (TL) with its entrance aperture oriented upward to measure the downward flux of gases at the lunar surface. The instrument was turned on December 27, 1971, 50 h after sunset, and operated throughout the lunar night. The advent of sunrise brought a high background gas level, thus operations were discontinued during lunar daytime except for a brief check near noon. Operation was resumed near sunset and continued throughout the nights for the second through ninth lunations. Details of the experiment are in the Final Report, NASA-CR-150946 (Hoffman, 1975).

The data from the LACE experiment were downloaded and archived at the NASA Space Science Data Coordinated Archive (NSSDCA). Our Monte Carlo models assuming a solar wind source reproduce the trend observed in the second and third lunations but not the magnitude. The trend seen in the fourth and fifth lunations is decreasing during the lunar night and cannot be reproduced unless the solar wind source is reduced or lost to the surface.

2. Data calibration

LACE measured mass per unit charge, thus there is an ambiguity between a mass with a single charge and an atom or molecule having double that mass which is doubly ionized. The LACE data were available for mass/charge (M/Q) 1 to 100, but the usable data are in the range 16–45 AMU/Q. For a given mass number a measurement was made every 13.5 min. The raw data are in counts per 0.6 s. The first task was therefore to calibrate the data. There is no available calibration for the LACE mass spectrometer data, however, a similar instrument was constructed and flown on the Pioneer Venus mission. The relative sensitivity graph attached below was constructed for that instrument on Pioneer Venus by integrating isotopic ratio errors (Donahue and Hodges, 1992). The available curve was used by Hodges et al. (1974) for Ar. We inserted lines to measure the transmission coefficients for mass 16 to 45 (Fig. 1). As the transmission coefficient increases, the ions/count decreases. In other words, the transmission is a function of the efficiency of the measurement. We calculated conversion scale for those ions that we wanted to include in this study. Given that the argon sensitivity was exactly 100 atoms/cc per data count (Hodges, personal communication) we derived a conversion scale using the ratio of their transmission coefficients as shown in Fig. 1 for the Pioneer Venus calibration. The ratios of transmission coefficients for masses 16 to 110 are shown in Fig. 1, and the ratios read off the curve are listed in Table 1. For example, m22_counts = (m22_trscoeff/m40transcoef) ∗ 100. Although this may not be a precise value, it is the best we could estimate from the Pioneer Venus curve. We note that because our analysis is not particularly sensitive to the exact numbers, but rather relative values, precise calibrations will not alter our conclusions. (See Table 2.)

First, if one assumes that M/Q = 22 is ^{22}Ne and is uncontaminated and M/Q = 20 contains both ^{20}Ne and HF, then the ^{20}Ne abundance is calculated given the known isotopic ratio of ^{22}Ne and ^{20}Ne where ^{20}Ne

* Corresponding author at: NASA Goddard Space Flight Center, Magnetospheric Physics/Code 695, Greenbelt, MD 20771, USA.
E-mail address: rosemary.killen@nasa.gov (R.M. Killen).

https://doi.org/10.1016/j.icarus.2019.04.018
Received 25 May 2018; Received in revised form 29 March 2019; Accepted 17 April 2019
Available online 18 April 2019

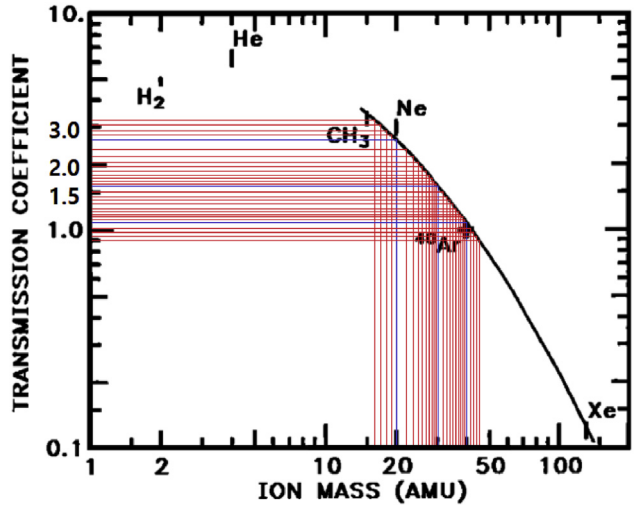

Fig. 1. Transmission coefficients used for ion mass to charge, M/Q, 1–100 AMU based on Pioneer Venus neutral mass spectrometer.

Table 1
Transmission coefficients for mass numbers 16–45.

Mass 16	3.1	Mass 26	1.8	Mass 36	1.2
Mass 17	3.0	Mass 27	1.7	Mass 37	1.1
Mass 18	2.9	Mass 28	1.7	Mass 38	1.1
Mass 19	2.7	Mass 29	1.6	Mass 39	1.1
Mass 20	2.5	Mass 30	1.6	Mass 40	1.05
Mass 21	2.2	Mass 31	1.5	Mass 41	1.0
Mass 22	2.1	Mass 32	1.4	Mass 42	1.0
Mass 23	2.0	Mass 33	1.4	Mass 43	0.9
Mass 24	2.0	Mass 34	1.3	Mass 44	0.9
Mass 25	1.9	Mass 35	1.2	Mass 45	0.9

Table 2
^{20}Ne densities estimated for lunations 2–5.

Lunation	Dates	^{20}Ne density
2nd	Jan. 24–Feb. 8, 1973	$(1.5 - 3.5) \times 10^3$ atoms/cm^3
3rd	Feb. 22–Mar. 9, 1973	$(2.0 - 4.5) \times 10^3$ atoms/cm^3
4th	Mar. 24–Apr. 8, 1973	$(2.0 - 4.0) \times 10^3$ atoms/cm^3
5th	Apr. 23–May 7. 1973	$(2.0 - 4.0) \times 10^3$ atoms/cm^3

is 90.48% of all Ne and ^{22}Ne is 9.25% of all neon (Grimberg et al., 2008). Given that the transmission coefficient of ^{22}Ne is 2.1 and the transmission coefficient of ^{20}Ne is 2.5, we derive that the sensitivity of ^{22}Ne is 50 atoms/count and the sensitivity of ^{20}Ne is 40 atoms/count. Examination of the LACE raw data (Supplemental material) shows there was significant background noise during the measurements of masses lower than ~ 35 amu. This noise ramped up with decreasing mass, and it was attributed to electronic disturbances from unshielded high voltage wires and collectors (Apollo 17 mission evaluation team). To this end, a mass 22 peak was identified at each 0.6 s integration period within the shifted mass range (25–26 amu). Then local minima about the peak were used to estimate the background contribution weighted more towards lower masses. The background contribution was then subtracted from the mass peak to calculate the ^{22}Ne density (see also Fig. 4 and 5). The corrected background subtracted counts in bin 22 vary from about 2–10. Hoffman (1975) used a similar approach to subtract the background noise, however they obtained counts more than an order of magnitude larger. The density of ^{20}Ne must be 9.78 times that for ^{22}Ne. We justify the assumption of contamination of the mass 20 bin by two lines of reasoning. First, the Rosetta Orbiter Spectrometer for Ion and Neutral Analysis (ROSINA) mass spectrometer onboard the Rosetta spacecraft continued to outgas for many years even

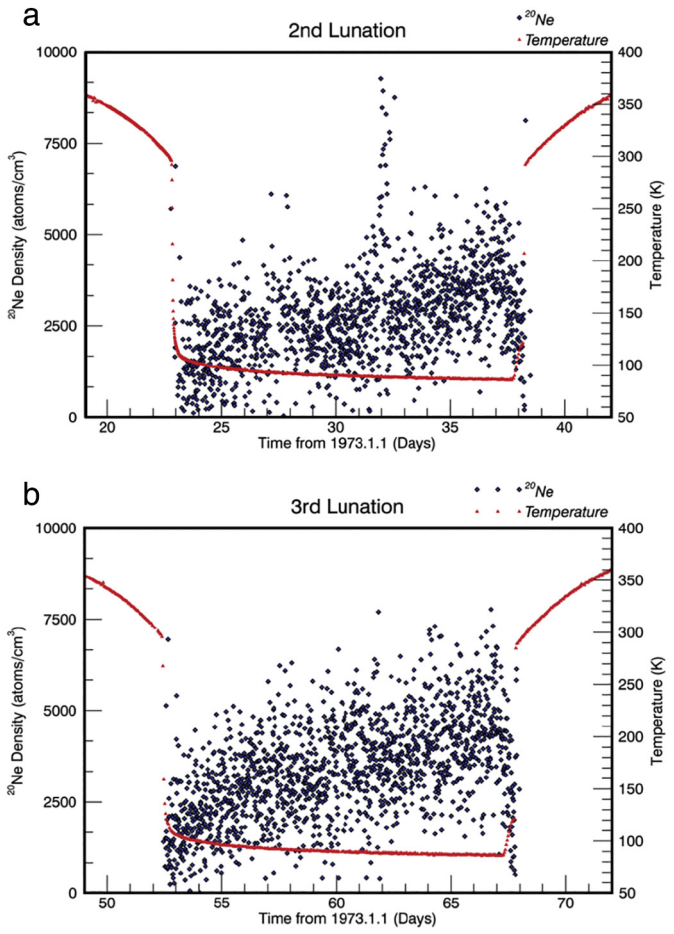

Fig. 2. The ^{20}Ne densities measured on the second (left) and third (right) lunations are plotted on the nightside from dusk to dawn (blue dots). The red lines are the temperature on the surface measured by the thermocouple placed as part of the ALSEP package. We determined dusk by the time the temperature dropped and dawn where the temperature suddenly rose.

in the cold outer solar system. Although the most important contaminant during the first 200 days of the mission was water, there is a strong peak at mass 19 corresponding to fluorine, reported to be an internal source (Schlappi et al., 2010).

3. Nightside Ne densities

Nightside densities were plotted from approximately dusk to dawn for four lunations, the second through the fifth in the LACE data. The surface temperatures were read from the thermocouple placed on the surface near the mass spectrometer. The data were measured every 0.6 s. We determined dusk to be the time when the temperature plummeted and dawn where temperature rose abruptly. The plots of neon density through the night for lunations 2 and 3 are shown in Fig. 2; those for lunations 4 and 5 are shown in Fig. 3.

The neon densities on the second and third lunations increase during the night from dusk to dawn. This is consistent with the results from Benna et al. (2015) and with theory of an exosphere in thermal equilibrium with the surface (Hodges, 1973). However, on the fourth and fifth lunations the neon density decreased from dusk to dawn. This is not consistent with previously published model results, but the measurement was also noted by Hodges et al. (1974).

4. Implication of solar wind impact for Neon

Neon is carried to the Moon with the solar wind. For normal solar

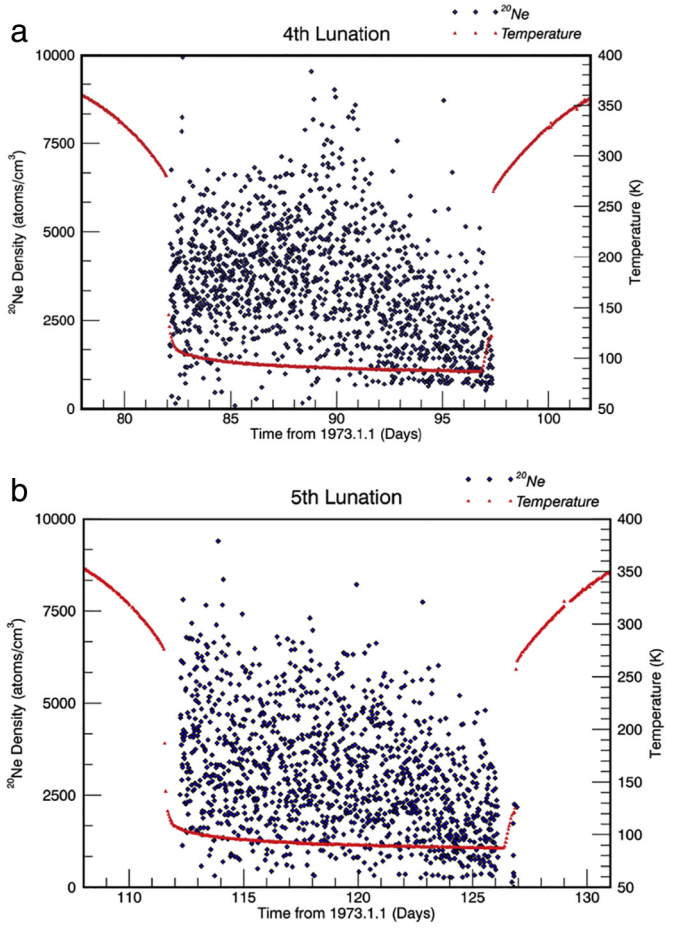

Fig. 3. The ^{20}Ne densities measured on the fourth (left) and fifth (right) lunations are plotted on the nightside from dusk to dawn (blue dots). The neon densities for these lunations decreased during the night, in contrast to the variation on the second and third lunations.

wind conditions near solar minimum, Ne/O = 0.17, O/H = 4.86×10^{-4} (Shearer et al., 2014). For normal slow wind speed (v_{sw} = 400 km/s) and density (N_{sw} = 5 cm^{-3}), the solar wind influx of ^{20}Ne is 8.2×10^{-5}(N_{sw} v_{sw}), or 1.6×10^{4} cm^{-2} s^{-1}. The solar wind composition in a Coronal Mass Ejection (CME) driver gas is given in Table 5 of von Steiger et al. (2000). The photoionization rate for Ne depends on the solar ionizing flux and is therefore dependent on the solar cycle. It is listed as 1.1×10^{-7} s^{-1} in 1978 and $5. \times 10^{-7}$ s^{-1} in 2002 (Bochsler et al., 2014). The solar cycle was approximately the same in 1972 as in 1978 except that in 1972 the solar cycle was in its declining phase and on 1978 the solar cycle was increasing. The Ne photoionization lifetime was thus about 9×10^{6} seconds, 100 days, or 3.4 months, for our observations.

Benna et al. (2015) measured the Ne abundance in the lunar exosphere with Lunar Atmosphere Dust and Environment Explorer (LADEE) Neutral Mass Spectrometer (NMS) during the Coronal Mass Ejection (CME) period of 7–27 Feb. 2014. The surface number density for Ne given by Benna et al. (2015) is $n_0 = 2 \times 10^{4}$ cm^{-3} about an order of magnitude more than our average value (2–4 $\times 10^{3}$) and that of Cook et al. (2013) (4.4×10^{3} cm^{-3}). Hodges et al. (1974) reported a nightside density of ^{20}Ne of 10^{5} cm^{-3} and a theoretical nightside density of 1.1×10^{5} cm^{-3} (Hodges, 1973) almost two orders of magnitude higher than our measured nominal value, (1.5–4.5) $\times 10^{3}$ atoms cm^{-3}. The Benna et al. (2015) value was reported to be observed during a CME. Because photoionization does not occur on the nightside, the average photoionization lifetime over the entire lunation should be multiplied by 2 in the analytical

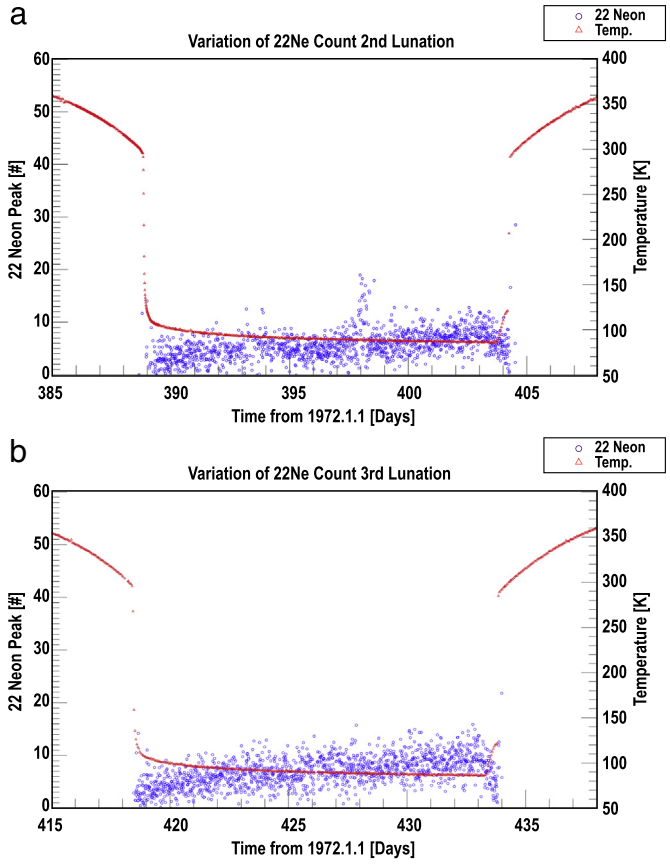

Fig. 4. ^{22}Ne counts for second and third lunations after background subtraction, which were used to estimate the true ^{20}Ne density.

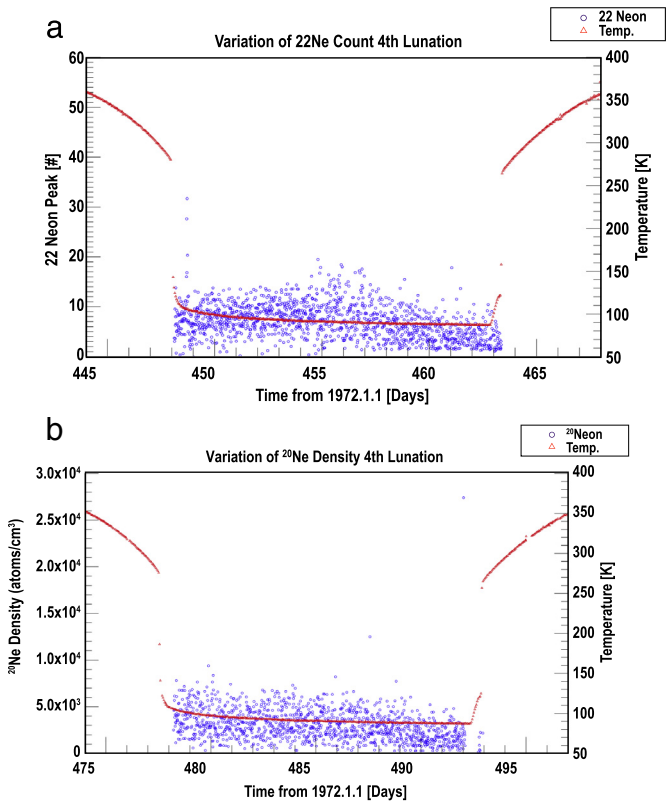

Fig. 5. ^{22}Ne counts for the fourth lunation after background subtraction (left), which were used to estimate the true ^{20}Ne density (right).

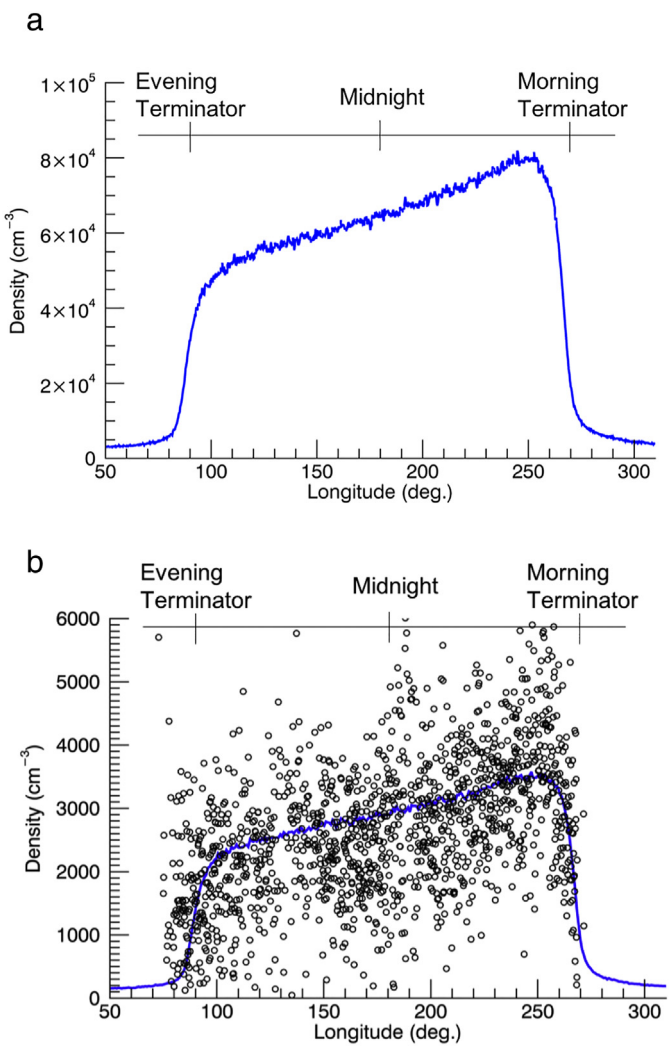

Fig. 6. Simulation (1) 6a and (2) 6b of neon density at TL using the averaged SW flux $N_{SW}v_{SW}$(Ne) = 1.65 × 10^4 $cm^{-2}s^{-1}$ and the photoionization lifetime of 100 days (a) and 4.5 days (b). We obtained a peak density of ~7.9 × 10^4 cm^{-3} and ~3800 cm^{-3} that occurred ~40 h before the dawn terminator (~250° longitude) for Simulation (1) and (2), respectively. Simulation (1) modeled result is consistent with Hodges et al. (1974) estimate of 1.1 × 10^5 cm^{-3}, which used a neon ion flux that was a factor of 1.5 larger. However, Simulation (2) using the artificial lifetime obtains results more consistent with LACE measurements during lunations 2 and 3, and the upper limit of densities observed near dawn by LAMP (Cook et al., 2013).

aproximation, so that the abundance in the exosphere depends on the solar wind flux over the preceding 6 months rather than 3 months. Because only lunar night time LACE observations were used, none of those observations were taken when the Moon was in the Earth's geomagnetic tail where the solar wind would not impact the lunar surface.

5. Model

We adapted the Monte Carlo model used in Tucker et al. (2015, 2019) in order to model the global concentration of neon in the Moon's exosphere. It is assumed that neon implanted by the solar wind is balanced by neon degassed from the surface. The computational domain is centered on the moon and discretized in spherical coordinates with a radial increment of 12 km and azimuthal and zenith increments of ~5 degrees. The moon is chosen as an inertial frame, and illumination of the surface is tracked assuming an average lunar day equivalent to 29.5 Earth days. For the model, the local surface temperature was estimated using T(Z) = 250 K ∗ $\cos^{1/4}$(Z) + 100 K, where Z is the solar zenith angle (Butler, 1997; Crider and Vondrak, 2002). The neon source flux from the soil on the illuminated hemisphere is assumed to be equivalent to the incident SW flux ^{20}Ne is 8.2 × 10^{-5}(N_{sw} v_{sw})cos(Z). Representative molecules are emitted isotropically from each surface element using the Maxwell Boltzmann Flux speed distribution at the local surface temperature with a cosine angular distribution to direct the velocities (Brinkmann, 1970). If a computational particle was traveling faster than the escape speed at radial distances above 1800 km it was removed from the simulation. However, thermal escape is negligible for neon, so the dominant loss mechanism was photoionization. When particles hit the surface, they are assumed to be accommodated to the surface temperature and diffusely scattered.

Three simulations were carried out in the analyses of the LACE measurements. To this end, we tracked the exosphere density at 20 degrees latitude as a function of lunation. The model data plotted in Fig. 6 were obtained by averaging the neon density within ½ a scale height of the surface at the TL latitude over time intervals of 1.5 h. Note we obtained a similar result using averages collected over a shorter 30-min time intervals, however to reduce the scatter due to model statistics we show the results obtained using the larger interval. Simulation (1) was carried out using the normal (averaged) solar wind flux of 8.2 × 10^{-5}(N_{sw} v_{sw})cos(Z) and the actual photoionization lifetime of 3.4 months, Fig. 6a. However, the predicted ^{20}Ne densities were over an order of magnitude larger than the LACE measurements. We found an exospheric lifetime of ~4.5 days for ^{20}Ne was required to obtain densities on the same magnitude as the LACE measurements shown in Simulation (2), Fig. 6b. Lastly, in Simulation (3) we consider temporal variations using OMNI data of the variable solar wind during lunations 2–5 with the lifetime of ~4.5 days. The results obtained in Simulation (3) are shown in the supplementary information.

6. Conclusions

The measured densities were consistent with the ^{20}Ne column densities reported by Cook et al. (2013) for normal conditions. This is an order of magnitude less than those reported by Benna et al. (2015) for CME conditions. Our Monte Carlo code employing the assumption of a 100 day photoionization lifetime and no surface adsorption results in densities a factor of 2–4 larger than the Benna et al. (2015) measurements. For CME conditions, the solar wind would have an enhanced abundance of heavy ions such that Ne/O = 0.32 and O/H = 3 × 10^{-4}. If v_{sw} = 800 km/s and N_{sw} = 10 cm^{-3} as expected for the CME, then the solar wind Ne flux to the lunar surface would be Ne = 7.7 × 10^4 $cm^{-2}s^{-1}$. However, using the actual photoionization lifetime of 100 days, and a nominal SW flux $N_{SW}v_{SW}$(Ne) = 1.65 × 10^4 $cm^{-2}s^{-1}$ the Ne density just before dawn would have been 8 × 10^4 cm^{-3} consistent with the theoretical result from Hodges (1973) and twice that of the night time peak reported by Benna et al. (2015), which was attributed to a CME passage.

Using the non-uniform surface temperature T(Z) = 250 ∗ cos (Z) + 100 K (e.g., Crider and Vondrak, 2002), where Z is the solar zenith angle, and applying the photoionization loss only on the dayside, the Monte Carlo model densities are a factor of ~20 larger at midnight compared to the LACE measurement. The OMNI data indicated the solar wind flux varied by a factor of ~10 on timescales of hours to days during the LACE experiment. When using the OMNI data with an artificial lifetime of ~4.5 days, the resulting ^{20}Ne densities varied by less than 50% from that obtained using normal average solar wind conditions.

We could not reproduce the trend of the densities from dusk to dawn as measured during the 4th and 5th lunations. During those lunations the ^{20}Ne density continued to decrease during the night, in contrast to lunations 2 and 3 where the densities increased during the night, consistent with cooling throughout the night. Apparently, explaining the ^{20}Ne distribution is not as simple as assuming dynamic

equilibrium with the solar wind and an exosphere accommodated to the local surface temperature. Furthermore, extracting the accurate abundance of Ne from in situ mass spectrometer data on the Moon remains an important topic of investigation. Neon is highly non-reactive so understanding its sources and sinks to the exosphere can directly inform us about the retention of atoms in the lunar regolith by physical defects and the energetics of space weather events.

An enhanced Ne measurement occurred during the night of 5th lunation when Taurus Littrow (TL) was located approximately 24–28 h from the morning terminator. Therefore, in the simulation approximately 38 h before TL rotated to dawn terminator the SW enhancement flux was elevated and the response of the exosphere was simulated. We initially thought that the increase in M/Q 22 at the end of the fifth lunation before sunrise might have been due to outgassing of a contaminant, possibly CO_2^{++} in the instrument near dawn or atoms hopping from the dayside to the nightside. However, if CO_2^{++} (M/Q = 22) is the result of ionization of CO_2^{+} (M/Q = 44) then the rise in 22 should have been 5% of the rise in M/Q = 44 due to the known fractionation. Instead the M22/M44 rise ratio was approximately 8.5.

We also see an increase in oxygen and hydroxyl at the same time as the increase in M/Q 22. The increased counts at dawn at mass 20 could be MgO^{++}, Ar^{++}or Ca^{++} as well as ^{20}Ne. However, the ratios of the measured species, which were measured as mass per charge, are strange and not consistent with fractionation due to expected isotopic ratios. If the counts in bin 20 are not contaminated, we can estimate the ^{20}Ne density by multiplying counts by 40, giving a ^{20}Ne density of about 1.4×10^4, fairly consistent with the sunrise ratio published by Benna et al. (2015) from LADEE data. In addition to the measured ratios of M/Q 22 and 44, we cannot model the decrease in M/Q 20 during the nightside for lunations 4 and 5. Therefore, we have shown that explaining the Ne distribution is not as simple as assuming dynamic equilibrium with the solar wind and an exosphere accommodated to the local surface temperature. This was also noted by Hodges et al. (1974), who conclude that the failure of the Apollo 17 data to rise late in the night may indicate a slight amount of adsorption. However, this does not explain the difference between lunations 2 and 3 and the lunations 4 and 5, respectively. We have shown that the enhanced solar wind flux cannot reproduce the observed rapid enhancement in Ne densities at dawn, and this is probably an artifact due to outgassing in the instrument.

Acknowledgements

RMK was supported by the DREAM2 Team of the NASA SSERVI Virtual Institute and by a grant from the NASA Solar System Observations program. OJT was supported by a NASA Postdoctoral Fellowship. SJK and JKP acknowledge support from the Space Core Technology program through NRF funded by the Ministry of Education, Science and Technology, Republic of Korea. We acknowledge use of NASA/GSFC's Space Physics Data Facility's OMNIWeb and OMNI data (King and Papatashvilli, 2018; Smith and Barnes, 2018). We used data from the IMP-6 spacecraft in Earth orbit during the years 1971–1974. The LACE data are being archived in the NASA Planetary Data System Geophysics Node.

Appendix A. Supplementary data

Supplementary data to this article can be found online at https://doi.org/10.1016/j.icarus.2019.04.018.

References

Benna, M., et al., 2015. Variability of helium, neon, and argon in the lunar exosphere as observed by the LADEE NMS instrument. Geophys. Res. Lett. 42 #10, 3723–3729, 2015. https://doi.org/10.1002/2015GL064120.

Bochsler, P. et al., (2014). Solar photoionization rates for interstellar neutrals in the inner heliosphere: H, He, O, and Ne. Astron. J. Suppl. 210 (12) 10 pp. doi:https://doi.org/10.1088/0067-0049/210/1/12.

Brinkmann, R.T., 1970. Departures from jeans escape rate for H and He in the Earth's atmosphere. Planet. Space Sci. 18, 449–478.

Butler, B.J., 1997. The migration of volatiles on the surfaces of Mercury and the Moon. J. Geophys. Res. 102 (E8), 283–291.

Cook, J. C., et al., 2013. New upper limits on numerous atmospheric species in the native lunar atmosphere. *Icarus* 225, 681–687, 2013.10.1016/j.icarus.2013.04.010.

Crider, D.H., Vondrak, R.R., 2002. Hydrogen migration to the lunar poles by solar wind bombardment of the Moon. Adv. Space Res. 30 (8), 1869–1874.

Donahue, T. and R. R. Hodges., 1992. Past and present water budget of Venus. *Journ. Geophys.Res.*97 E4, 6083–6091, 1992 doi: https://doi.org/10.1029/92JE00343.

Grimberg, A, H. Baur, F. Buhler, P. Bochsler, and R. Wieler. 2008. Solar wind helium, neon, and argon isotopic and elemental composition: Data from the metallic glass flown on NASA's Genesis mission. *Geochim. Cosmochim. Acta* 72, 626–645, 2008. Doi: https://doi.org/10.1016/j.gca.2007.10.017

Hodges, R. R. Helium and hydrogen in the lunar atmosphere. J. Geophys. Res. 78, 8055, 1973.ODGES, R. R., HOFFMAN, J.

Hodges, R.R., Hoffman, J.H., Johnson, F.S., 1974. The lunar atmosphere. Icarus 21, 415–426.

Hoffman, J. H., 1975. Lunar Atmospheric Composition Experiment Final Report. NAS 9-12074, June 1, 1971- September 30, 1975.

King, J.H., Papatashvilli, N., 2018. Plasma data from cohoweb. *CDAWeb*, Adnet Systems, NASA Goddard Space Flight Center, Greenbelt MD. Generated(Feb. 15, 2018).

Schlappi, B., Altwegg, K., Balsiger, H., et al., 2010. Influence of spacecraft outgassing on the exploration of tenuous atmospheres with in situ mass spectrometry. J. Geophys. Res. Space Phys. 115 (A12). https://doi.org/10.1029/2010JA015734.

Shearer, P., et al., 2014. The solar wind neon abundance observed with ACE/SWICS and Ulysses/SWICS. Astrophys. J. 789 (1), 60. https://doi.org/10.1088/0004-637X/789/1/60.

Smith, E. J., A. Barnes, 2018. *CDAWeb*, NASA JPL/AMES.

von Steiger, R., N. A. Schwadron, L. A. Fisk, J. Geiss, S. Hefti, B. Wilken, R. F. Wimmer-Schweingruber, and T. H. Zurbuchen. 2000. Composition of the quasi-stationary solar wind flows from Ulysses/solar wind ion composition spectrometer, J. Geophys. Res., 105(A12), 27,217–27,238, doi:https://doi.org/10.1029/1999JA000358.

Tucker, O.J., Johnson, R.E., Young, L.A., 2015. Gas transfer in the Pluto-Charon system: a Charon atmosphere. Icarus 246, 291–297.

Tucker, O. J., Farrell, W. M., Killen, R. M., & Hurley, D. M. (2019). Solar wind implantation into the lunar regolith: Monte Carlo simulations of H retention in a surface with defects and the H2 exosphere. J. Geophys. Res. Planets, 124, 278–293. doi: https://doi.org/10.1029/2018JE005805.